Deployable Multi-faceted Reflectarray Antenna in Offset Configuration with Band Enhancement

Borja Imaz-Lueje, *Student Member, IEEE*, Marcos R. Pino, and Manuel Arrebola, *Senior Member, IEEE*

Abstract—A multi-faceted reflectarray that follows a parabolic cylinder structure is presented to improve the antenna bandwidth compared to a conventional reflectarray. The antenna is suitable to be used in SmallSats since it is low-profile and low-cost and can be easily folded and deployed on this kind of platform. To evaluate the characteristics of this solution as well as the ability to work in different polarizations, two multi-faceted demonstrators have been designed, manufactured, and tested. They generate a pencil beam pattern in Ka-band and are compared to a single facet offset reflectarray of equivalent aperture size. The multi-faceted structure conveniently exploits both the unit cell properties as well as the geometry to achieve a significant improvement in antenna bandwidth compared to the single facet version, with a better trade-off between antenna characteristics and performance achieved.

Index Terms— reflectarray antennas, multi-faceted reflector, Ka-band antennas, satellite antennas.

I. INTRODUCTION

REFLECTARRAYS have attracted the interest of the scientific community in recent years. This type of antenna is typically based on a planar surface composed of an array of radiating elements [1]. This surface, which is spatially fed, collimates the power reflected in a direction (pencil beam) or defines a shaped beam. Due to their mechanical properties and array nature, reflectarrays have been positioned as an antenna candidate in many applications, such as cellular networks [2], RFID [3], or measurement systems [4], among others.

In particular, the satellite communications sector has been one of the main supporters of this type of antennas. The interest in using printed reflectarrays in satellite communications comes from their advantages over other traditional antennas, such as arrays or bulky parabolic reflectors [5]. Reflectarrays can generate beam-steering or multi-beam patterns [6]–[8], providing higher aperture efficiencies compared to arrays. In addition, they can also achieve shaped-beam patterns required in applications with very tight requirements, such as Direct Broadcast Satellite mission (DBS) [10]–[12] or some mega-constellation systems [13]. Apart from their electromagnetic

capabilities, reflectarrays are an interesting alternative to parabolic reflectors due to their low profile and better integration onboard the satellite. Based on microstrip technology, inflatable or deployable reflectarrays [14]–[19] were proposed to achieve large apertures antennas which can be easily stowed in a small volume during the launch. After the deployment process, the surface extends outside the spacecraft body while the feed is integrated into the satellite. The physical characteristics of deployable reflectarrays are especially interesting for some CubeSats missions, which require high gain beam pattern antennas under severe physical and weight constraints. The use of deployable reflectarrays has been successfully implemented in some space missions. NASA's MarCO [16] and ISARA [17] missions employ folded panel reflectarrays with a gain of about 30 dBi. Deployable reflectarrays have also been proposed for SAR missions [18],[19], where radiation patterns with narrow beam patterns are also sought. However, in all these cases, the panels are aligned in a single plane after the deployment. Therefore, the antenna works as an equivalent single facet reflectarray.

In contrast, printed reflectarrays usually have an inherent narrow bandwidth [20] mainly due to two factors: the bandwidth of the radiant elements and the spatial phase delay effect. Cell bandwidth is especially critical for moderate electrical size reflectarrays and depends mainly on the behavior of the phase element response when varying its physical dimensions [1]. The other factor, the spatial phase delay, is produced by the different path lengths between feed and reflector. The radiating elements are designed to compensate for the phase delay produced in each path at central frequency. However, as the frequency varies, so does the phase delay on each path. Usually, this phase change is not matched with the phase provided by the radiating elements which produce phase errors and, therefore, a degradation of the pattern in-band. The differential spatial phase delay is the predominant effect on pattern degradations in electrically large reflectarrays [21].

In the literature, there are several strategies focused on mitigating these issues. At the element level, multi-resonant cell topologies, consisting of single [22] or multiple stacked layers [21], have shown a considerable improvement in the element bandwidth. In addition, true time-delay cells with a large phase-shift range are also proposed as an element solution to reduce the spatial phase delay effect [23]. An improvement in the antenna bandwidth can also be achieved through optimization techniques that use the dimension of the elements as variables
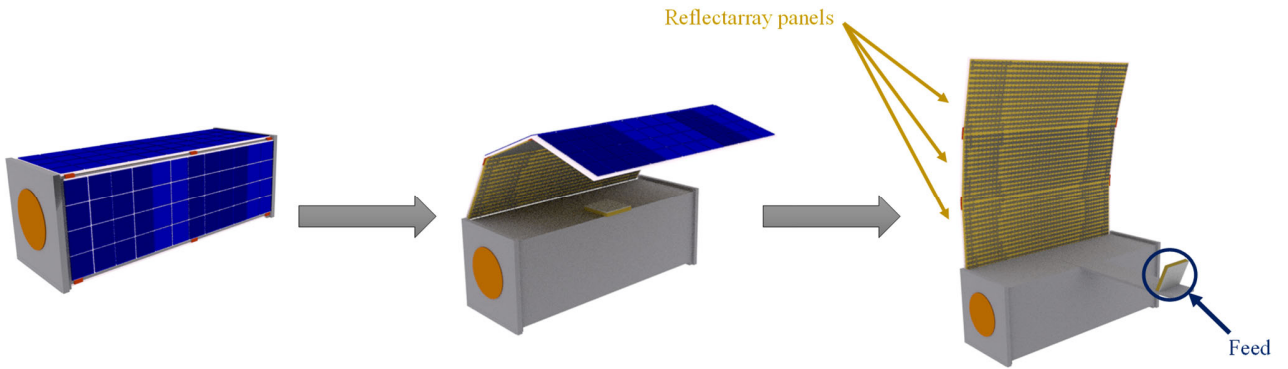
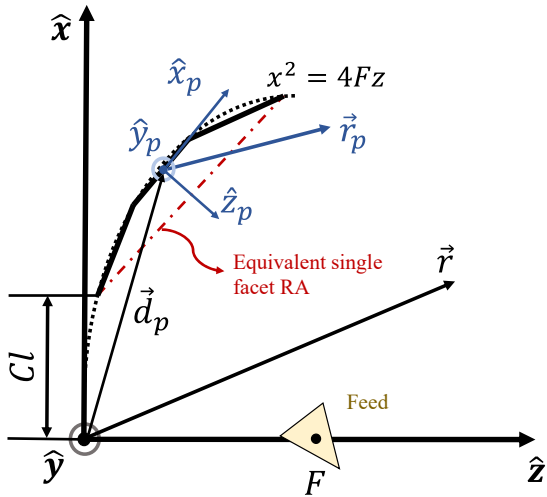Fig. 1. Proposed integration of multi-faceted reflectarrays onboard a SmallSat. Deployment system in-orbit.

Fig. 2. Optics of the multi-faceted structure. The reflectarray panels are in chordal planes of an equivalent parabola (dotted black line), which are defined in the general coordinate system $(\hat{x}, \hat{y}, \hat{z})$. Each panel is characterized from its unit vectors $(\hat{x}_p, \hat{y}_p, \hat{z}_p)$ and the position of its center, expressed with the vector $\vec{d}_p$.

[24]. According to the antenna optics, the increase of the f/D ratio reduces the difference between paths, but this leads to larger antenna dimensions and therefore bulkier structures. Alternatively, parabolic [25], or multi-faceted reflectarrays [26]-[28] can reduce considerably the errors associated with the differential spatial phase delay because their structure better resembles a parabola. Multi-faceted reflectarrays can improve the antenna performance in-band without increasing excessively the mechanical complexity of the structure. In fact, the 1-D multi-faceted configurations [28] can be perfectly adapted to the deployment systems used in satellites as [16] or [17].

In this work, a multi-faceted reflectarray is proposed to improve the in-band performance of a conventional reflectarray for its use in Smallsat platforms. The antenna structure consists of a single-offset configuration of panels that sectorize the equivalent parabola along the offset axis. Each panel is composed of simple topology cells used in other contributions such as [4],[29],[30], and [31]. To assess the performance of this antenna, two single-polarization multi-faceted prototypes are designed, evaluated, and tested. Both reflectarray structures can be used as a deployable antenna onboard a SmallSat (see Fig. 1) with identical optics but working in two different orthogonal polarizations. Besides, a single facet reflectarray is designed, manufactured, and tested to be used as a reference. According to the results achieved, the multi-faceted structures generate a beam more stable in-band in comparison with the single facet reflectarray. Some mismatches have been identified between the simulation and measured results in the multi-faceted prototypes. In this sense, an analysis of discrepancies is carried out to identify the most critical points in the manufacturing process. According to the results reported in this work, the multi-faceted structures achieve a significant bandwidth improvement compared to the one facet reflectarray, exploiting efficiently both the cell properties and the geometry of the antenna. Besides, the similar behavior observed in both multi-faceted antennas demonstrates their ability to work in dual-polarization.

II. ANALYSIS OF MULTI-FACETED REFLECTARRAYS

The proposed multi-faceted reflectarray structure onboard a SmallSat is shown in Fig. 1. Antenna panels can be folded according to the spacecraft body during the launch. Once the satellite is in orbit, the lower panel is adjusted parallel to one of the satellite sides while the rest are positioned accordingly to conform a parabolic structure.

A. Optics Definition.

The side view of the deployed reflectarray is shown in Fig. 2. In general, it can be composed of N panels placed in chordal planes of an equivalent parabolic model. The parabola is defined on the offset plane XZ according to the antenna coordinate system $(\hat{x}, \hat{y}, \hat{z})$. The main parameters of this model are the focal distance (F) and the clearance (Cl).

Each panel is characterized by its local coordinate system $(\hat{x}_p, \hat{y}_p, \hat{z}_p)$ with $\hat{z}_p$ normal to the panel, and the position vector defining the origin of this system $\vec{d}_p$. The coordinate system of each panel is directly related to the general coordinate system according to a 3x3 matrix composed of the unit vectors $(\hat{x}_p, \hat{y}_p, \hat{z}_p)$ of the panel.
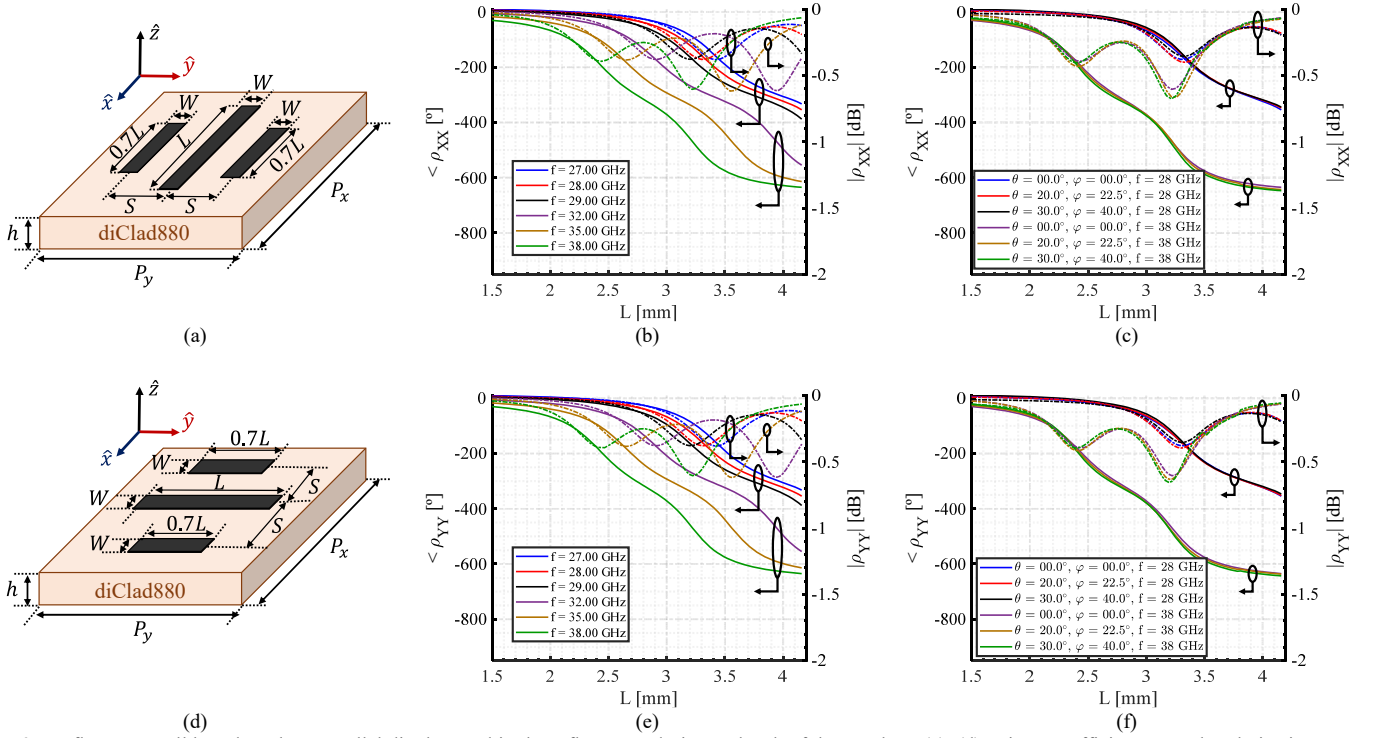
Fig. 3. Reflectarray cell based on three parallel dipoles used in the reflectarray designs: Sketch of the topology (a), (d); Direct coefficient on each polarization as a function of L (length of the central dipole) at different frequencies under normal incidence (b), (e); Direct coefficient on each polarization as a function of L under
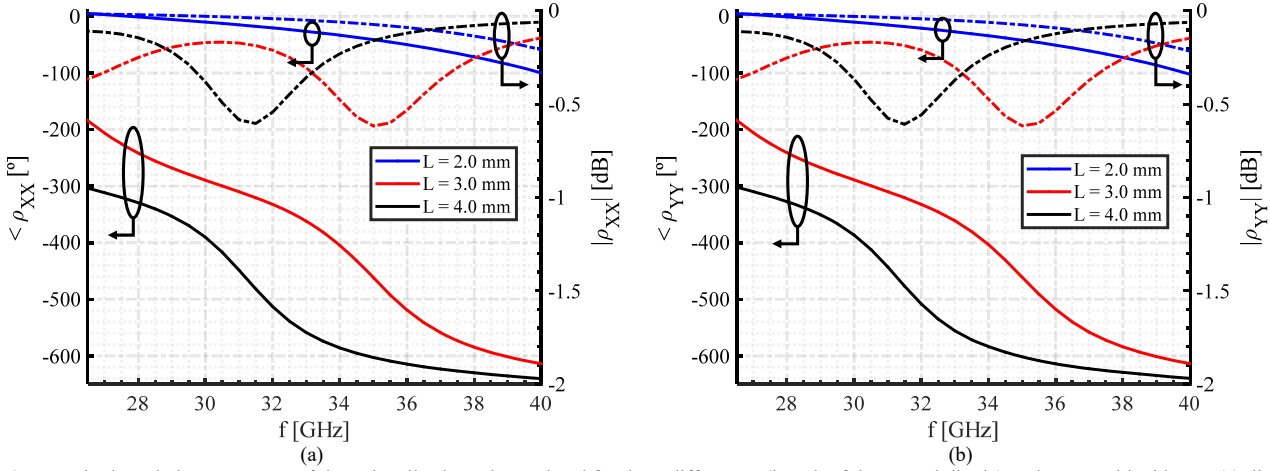

Fig. 4. Magnitude and phase response of the unit cells along the Ka-band for three different L (length of the central dipole) under normal incidence: (a) direct coefficient ρ_{XX} of the cell used in the SFRA and MFRAX; (b) direct coefficient ρ_{YY} of the cell used in the MFRAY.

A primary feed is placed at the focal point F to illuminate the reflectarray, which produces an incident field on its surface. According to the single-offset configuration, the feed is tilted with regard to the Z-axis of the general coordinate system.

B. Analysis of the reflectarray panel.

Each reflectarray panel is comprised of reflective elements designed to modify the incident field on the flat surface to obtain a given reflected field that generates the desired radiated pattern. The relation between the reflected and incident fields on the reflectarray panel can be expressed as:

$$\vec{E}_{ref}(\vec{r}_p^i) = \mathbf{R}^i \vec{E}_{inc}(\vec{r}_p^i) = \begin{pmatrix} \rho_{XX}^i & \rho_{XY}^i \\ \rho_{YX}^i & \rho_{YY}^i \end{pmatrix} \vec{E}_{inc}(\vec{r}_p^i) \qquad (1)$$

where $\vec{E}_{ref}(\vec{r}_p^i)$ and $\vec{E}_{inc}(\vec{r}_p^i)$ are the tangential components of the reflected and incident field in the i-th unit cell of the panel; $\vec{r}_p^i$ are the coordinates of the unit cell expressed in the panel coordinate system; and $\mathbf{R}^i$ is the matrix of reflection coefficients whose elements are classified into direct coefficients (ρ_{XX}^i and ρ_{YY}^i) and cross-coefficients (ρ_{XY}^i and ρ_{YX}^i). $\mathbf{R}^i$ matrix characterizes the behavior of the unit cell and is obtained using a Method of Moments considering Local Periodicity (MoM-LP) [31].

On the other hand, the farfield of the p-th panel $\vec{E}_p = E_{\theta,p}\hat{\theta}_p + E_{\varphi,p}\hat{\varphi}_p$ is obtained according to the second principle of equivalence [32],
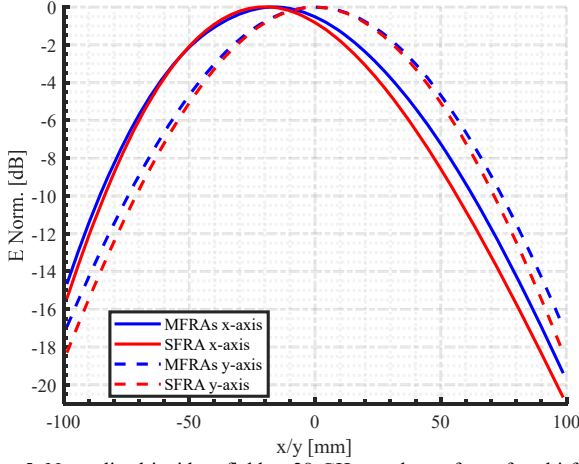
Fig. 5. Normalized incident field at 28 GHz on the surface of multi-faceted reflectarrays (MFRAs) and single facet reflectarray (SFRA) designs. Solid lines correspond with the main cut along the x-axis and dotted with the main cut along the y-axis.

$$E_{\theta,p}(\vec{r}_p) = jk_0\eta_0 \frac{\exp(-jk_0 r_p)}{2\pi r} (P_x \cos\varphi_p + P_y \sin\varphi_p) \quad (2)$$

$$E_{\varphi,p}(\vec{r}_p) = -jk_0\eta_0 \frac{\exp(-jk_0 r_p)}{2\pi r} \cos\theta_p \left(P_y \cos\varphi_p - P_x \sin\varphi_p \right) \quad (3)$$

where $E_{\theta,p}$, $E_{\varphi,p}$ are the spherical components of the farfield radiated by the p-th panel, regarding its local coordinate system; k_0 is the propagation constant in vacuum; $\eta_0 = 120\pi\ \Omega$ is the vacuum impedance; $(r_p, \theta_p, \varphi_p)$ are the spherical coordinates expressed in the panel coordinate system for a given direction; and $P_{x/y}$ the spectrum functions calculated by the integration of the reflected tangential electric field [32].

C. Farfield of the multi-faceted structure.

The total radiated farfield of the structure $\vec{E} = E_\theta \hat{\theta} + E_\theta \hat{\varphi}$, is calculated as the sum of the contribution field of each panel,

$$\vec{E}(\vec{r}_a) = \sum_{p=1}^{N} \vec{E}_p(\vec{r}_a) \quad (4)$$

where $\vec{r}_a$ indicates the direction of space expressed in an arbitrary coordinate system, and $\vec{E}_p(\vec{r}_a)$ is the radiated field vector of each panel expressed in the same coordinate system. In the antennas proposed in this paper, the general coordinate system (see Fig. 2) is taken as a reference to apply the sum of field contributions ($\vec{r}_a = \vec{r}$).

III. DESIGN OF MULTI-FACETED REFLECTARRAY

To evaluate the performance of the proposed structure, in this paper two multi-faceted reflectarrays (MFRAs) working in X-polarization (MFRAX) and Y-polarization (MFRAY) respectively are designed in Ka-band at 28 GHz. The antennas generate a pencil-beam pattern in the broadside direction regarding the general coordinate system depicted in Fig. 2. A

single facet reflectarray (SFRA) working in X-polarization with an equivalent aperture to the multi-faceted structures is designed to take it as the reference during the evaluation of the performance.

A. Cell Characterization.

Fig. 3(a) and (d) show the unit cells considered in this work. The first is used in the SFRA and the MFRAX while the second topology is used in the MFRAY. The radiating element in both cells consists of a single layer rectangular cell composed of three metallic dipoles, which have a width (W) of 0.5 mm and have separated each other $S = 1.43$ mm. The ratio between the length of the central dipole and the lateral ones is 0.7. The dipoles are printed on the top layer of the substrate diClad 880 ($\varepsilon_r = 2.26$, $\tan\delta = 0.0025$) of thickness $h = 0.762$ mm. The dipoles are aligned with one axis of the reflectarray panel (x axis in the first cell topology and y axis in the second). The periodicity of the cell is 4.29 mm on both axes ($P_x = P_y$), which corresponds with $0.4\lambda_0$.

Fig. 3(b) and (e) show the behavior in-band of the direct coefficient in each case when varying the length of the central dipole L considering normal incidence. The cells provide a quasi-linear phase-shift dependence with L in 2 GHz bandwidth, and a phase range of about a full cycle (360º). The losses introduced by the unit cells are lower than 0.4 dB, which means that more than 90% of the incident energy is effectively reflected. Besides, both cell topologies have good behavior at higher frequencies of the Ka-band, reaching a phase range up to 500º at the highest ones of the band (38 GHz). At this frequency, the unit cells still show low losses. This behavior can also be seen in Fig. 4, which shows the response of the cells in the entire Ka-band, for three different L. As the frequency increases, the phase difference between the minimum and maximum L increases, while the losses remain below 0.6 dB. Fig. 3(c), (f) shows the behavior of the cells under different angles of incidence at 28 and 38 GHz. The radiant elements demonstrate good angular stability in both magnitude and phase at the design frequency and upper frequencies of the Ka-band.

B. Antenna Optics.

The MFRAs is made up of 3 panels identical in size. Each one has 675 elements distributed in a rectangular grid of 15 x 45. Each panel is positioned according to the single-offset configuration of Fig. 2, where a focal distance (F) of 190 mm and a clearance (Cl) of 60 mm are considered. On the other hand, the SFRA is formed by 2025 elements (45 x 45 on each axis) with the same optics as shown in Fig. 2. The f/D ratio in both cases is approximately 1.0.

A Narda 665-20 pyramidal horn antenna is used to illuminate both reflectarrays. The horn is placed at the focus of the parabola and tilted 36.36º regarding the z-axis of Fig. 2. During the analysis and design processes, the pattern of the feed is ideally modeled as a $\cos^q\theta$ with a different q for each main cut, so the beamwidth in both planes is the same as the real horn antenna. Fig. 5 shows the taper in main planes for MFRAX and for the SFRA at 28 GHz, where the q factor is 21.0 and 19.7 in each main plane of the feed. The illumination taper is lower than
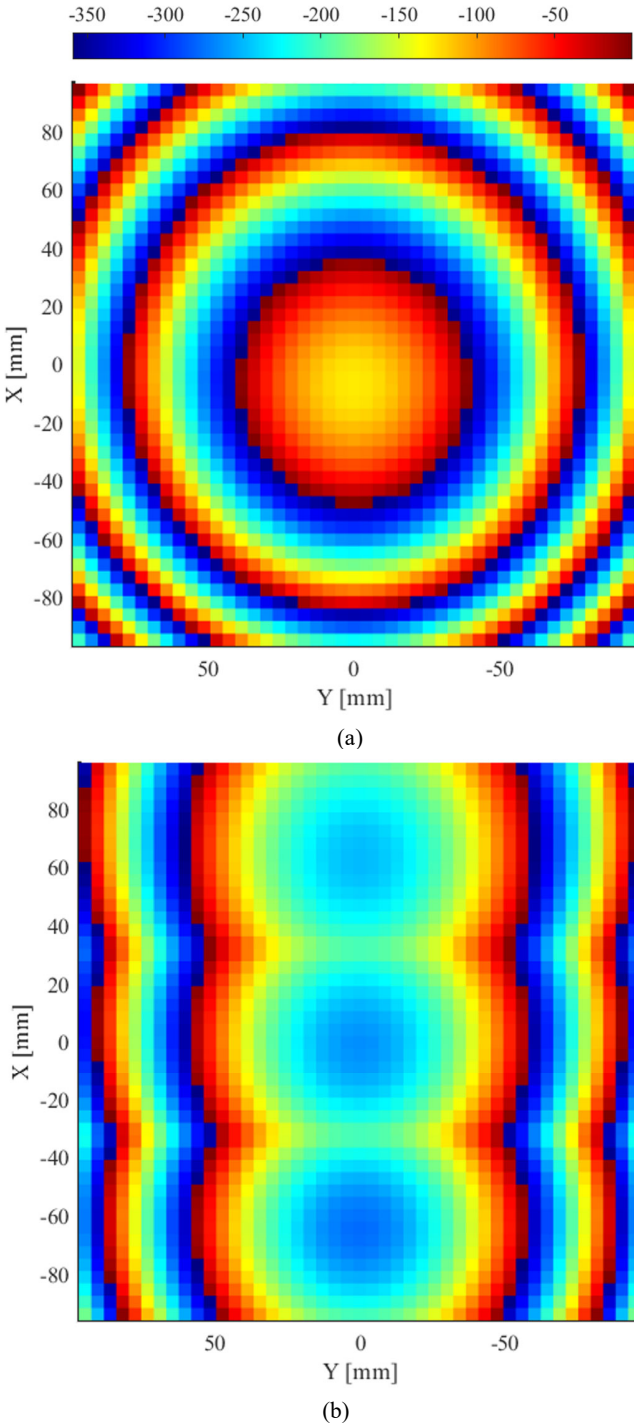
Fig. 6. Planar representation of the phase distribution in degrees [º] required in each design: (a) SFRA; (b) MFRAs.
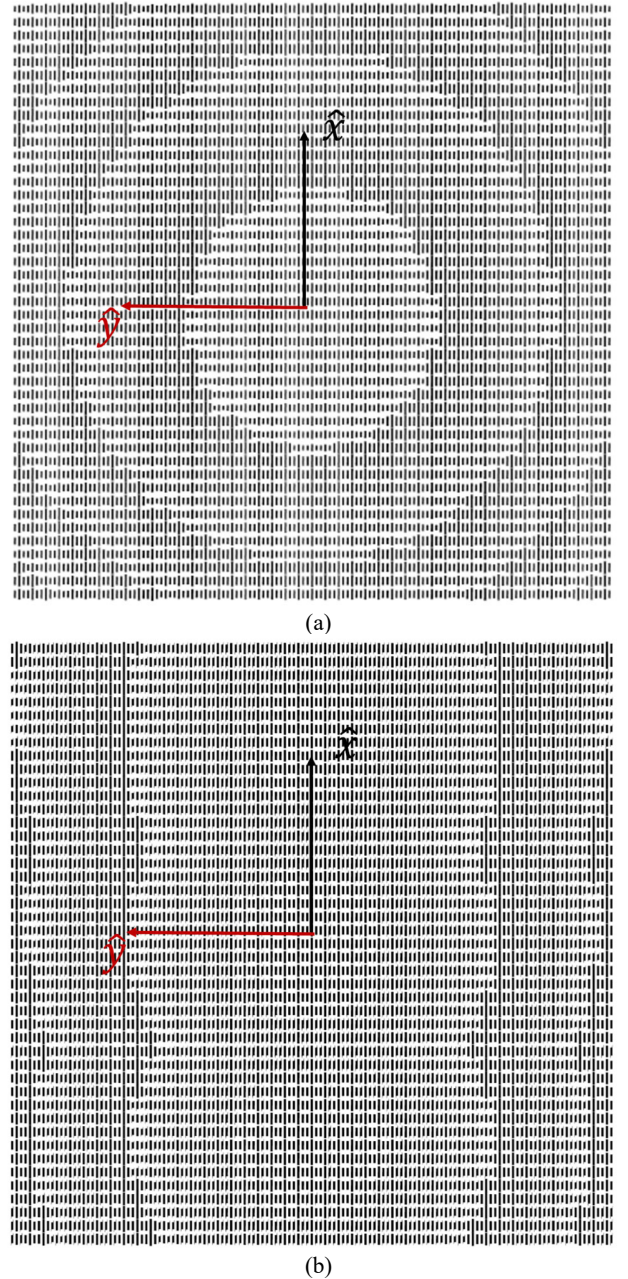

Fig. 7. Reflectarray layouts achieved: (a) SFRA; (b) MFRAX. The x- and y-axes are referred to the coordinate system of the central panel in each case.

-15 dB at the edges of the antenna, which ensures low spillover in both designs. The MFRAY has a similar taper to the MFRAX case which anticipates similar gain and aperture efficiency in both antennas. The SFRA has a slightly lower taper because of the optics of the antenna.

C. Reflectarray layouts design procedure.

According to array theory, to collimate a pencil beam in a certain direction (θ_0, φ_0) each reflectarray element must introduce a phase-shift calculated as [1],

$$\phi(x_i, y_i, z_i) = k_0[d_i - (x_i \sin \theta_0 \cos \varphi_0 + y_i \sin \theta_0 \sin \varphi_0 + z_i \cos \theta_0)] \quad (5)$$

where (x_i, y_i, z_i) are the coordinates of the i-th element of the reflectarray panel in a given coordinate system; and d_i is the distance from the phase center of the feed to the i-th element. This equation is independent of the used coordinate system, provided that the definition of all parameters is consistent. Considering the general coordinate system (see Fig. 2), the phase distributions of all antennas are computed to produce a pencil beam in the broadside direction $(\theta_0 = \varphi_0 = 0)$. The phase distribution achieved in the SFRA and the MFRAs is shown in Fig. 6. Along the sectorization x-axis, the MFRAs
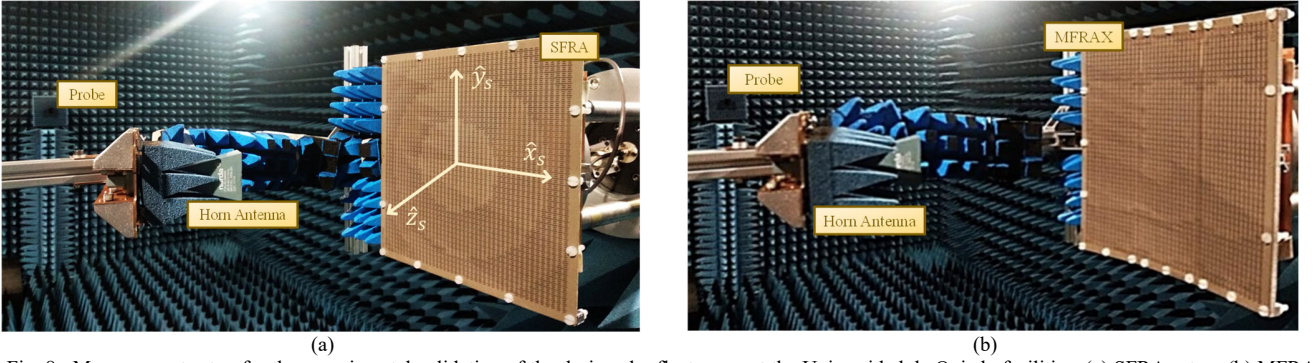
Fig. 8. Measurement setup for the experimental validation of the designed reflectarrays at the Universidad de Oviedo facilities: (a) SFRA setup; (b) MFRAX setup. The measurement is achieved considering the coordinate system of the unique panel of the antenna $(\hat{x}_s, \hat{y}_s, \hat{z}_s)$ in (a) and the coordinate system of the central panel $(\hat{x}_2, \hat{y}_2, \hat{z}_2)$ in (b).

TABLE I.   ANTENNA RF PERFORMANCE MEASURED. RANGE 25-31 GHz

		Single Facet Reflectarray (SFRA)					Multi-Faceted Reflectarray Pol X (MFRAX)					Multi-Faceted Reflectarray Pol Y (MFRAY)				
Frequency [GHz]		25.0	27.0	28.0	29.0	31.0	25.0	27.0	28.0	29.0	31.0	25.0	27.0	28.0	29.0	31.0
SLL [dB]	Az	-18.9	-26.9	-26.6	-22.3	-18.0	-10.2	-18.2	-20.9	-18.6	-13.1	-10.5	-17.6	-24.9	-20.4	-14.7
	El	-18.8	-23.3	-26.0	-21.1	-19.1	-19.7	-16.8	-19.4	-22.9	-18.3	-21.9	-18.0	-17.7	-18.8	-21.6
XP [dB]		-34.9	-40.1	-46.5	-48.4	-39.1	-33.3	-30.8	-30.0	-30.0	-31.4	-41.0	-35.9	-33.5	-32.5	-33.1
Eff. Ap. [%]		67.0	61.2	60.5	57.9	53.4	69.8	64.4	63.8	61.2	56.8	69.3	63.9	63.3	60.7	56.3
Gain [dBi]		30.0	32.2	32.9	32.5	31.6	29.6	32.0	32.3	32.4	31.6	29.5	31.9	32.1	32.2	31.9

structure has a smoother variation of the phase-shift than the SFRA configuration. Actually, the required phase-variation in cut $y = 0$ is 80º, much lower than a full cycle (360º). The multi-faceted optics in the sectorization axis compensates part of the phase-shift required for the element because of its closer similarity to a parabola. In the non-sectorized y-axis, similar behavior is achieved in both designs.

The same design procedure is applied to the 3 different layouts. The radiant elements are properly designed according to the phase distribution in Fig. 6 and the cell behavior depicted in Fig. 3 for each antenna. The design process is carried out element by element, using the mentioned MoM-LP [31] considering the real incidence angle of each cell. Therefore, the layouts of the SFRA and MFRAX are shown in Fig. 7. Being based on the same phase distribution, the unit cells in the MFRAY layout have similar relative size to that shown in the MFRAX case, but the dipoles are aligned with the y-axis of each panel.

The performance of all reflectarrays is assessed according to the analysis described above. The reflected field by each panel is calculated from (1) assuming the incident field depicted in Fig. 5. The $\boldsymbol{R}^i$ matrix is obtained from the layouts of each design applying MoM-LP. Once the reflected field is calculated, the partial farfields of each panel and the total farfield of the structure are computed using (2), (3), and (4) respectively. The simulated results are shown in comparison with the measured farfield patterns in section IV.

IV. EXPERIMENTAL VALIDATION.

The 3 designed reflectarrays have been manufactured and tested in the facilities of the University of Oviedo. The measurement setups for the SFRA and MFRAs are shown in Fig. 8. The MFRAX and MFRAY share the same supporting structure with a 90º rotation of the feed for the proper polarization in each case. For measurement purposes, the SFRA orientation is referred to its single panel meanwhile the MFRAs orientation is referred to their respective central panels. Since the referred panels have different orientations, the general coordinate system detailed in Fig. 2 is used to present the results.

The antenna prototypes have been measured using a spherical acquisition anechoic chamber. The antenna under test is located at 5 m from the antenna probe, which was a Ka-band standard gain horn. The proposed configuration implies that the probe is in the near field region of the reflectarrays. Therefore, an NF-FF transformation using the SNIFT software of TICRA [33] is carried out to obtain the farfield patterns.

A. Multi-faceted vs. Single Facet Antennas Performance.

Fig. 9 shows the measured and simulated radiation pattern in a 6 GHz bandwidth (25 – 31 GHz), considering the general coordinate system. Besides, Table I lists the main parameters of the farfield measured.

According to Fig. 9, a good agreement between simulations and measurements is achieved for the SFRA prototype as well
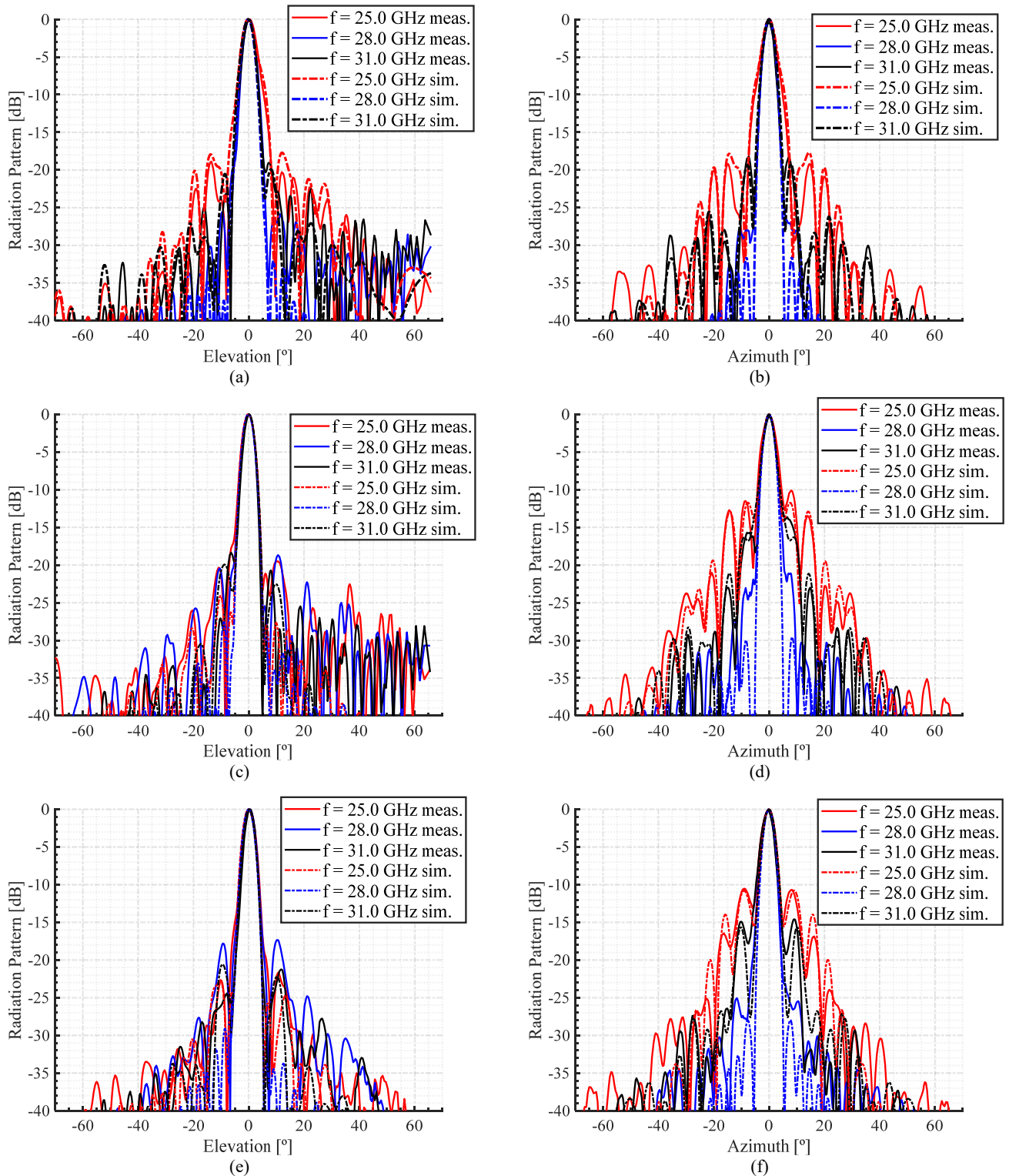
Fig. 9. Main cuts of the normalized radiation pattern in simulation and measurements for (a), (b) SFRA; (c), (d) MFRAX and (e), (f) MFRAY designs. Pattern from 25 to 31 GHz. The diagram pattern is expressed in the general coordinate system in all cases.

as for the multi-faceted prototypes in its azimuth cut (elevation = 0º). Regarding the elevation cut (Fig. 9(a),(c), and (e)), it is achieved a good agreement in the three antennas around the main beam, although the measured field values outside it are

higher than those predicted in the simulation.

Comparing the shape pattern of the prototypes the main beam of the MFRAs in elevation remains stable along the analyzed bandwidth while the SFRA suffers significant distortions,
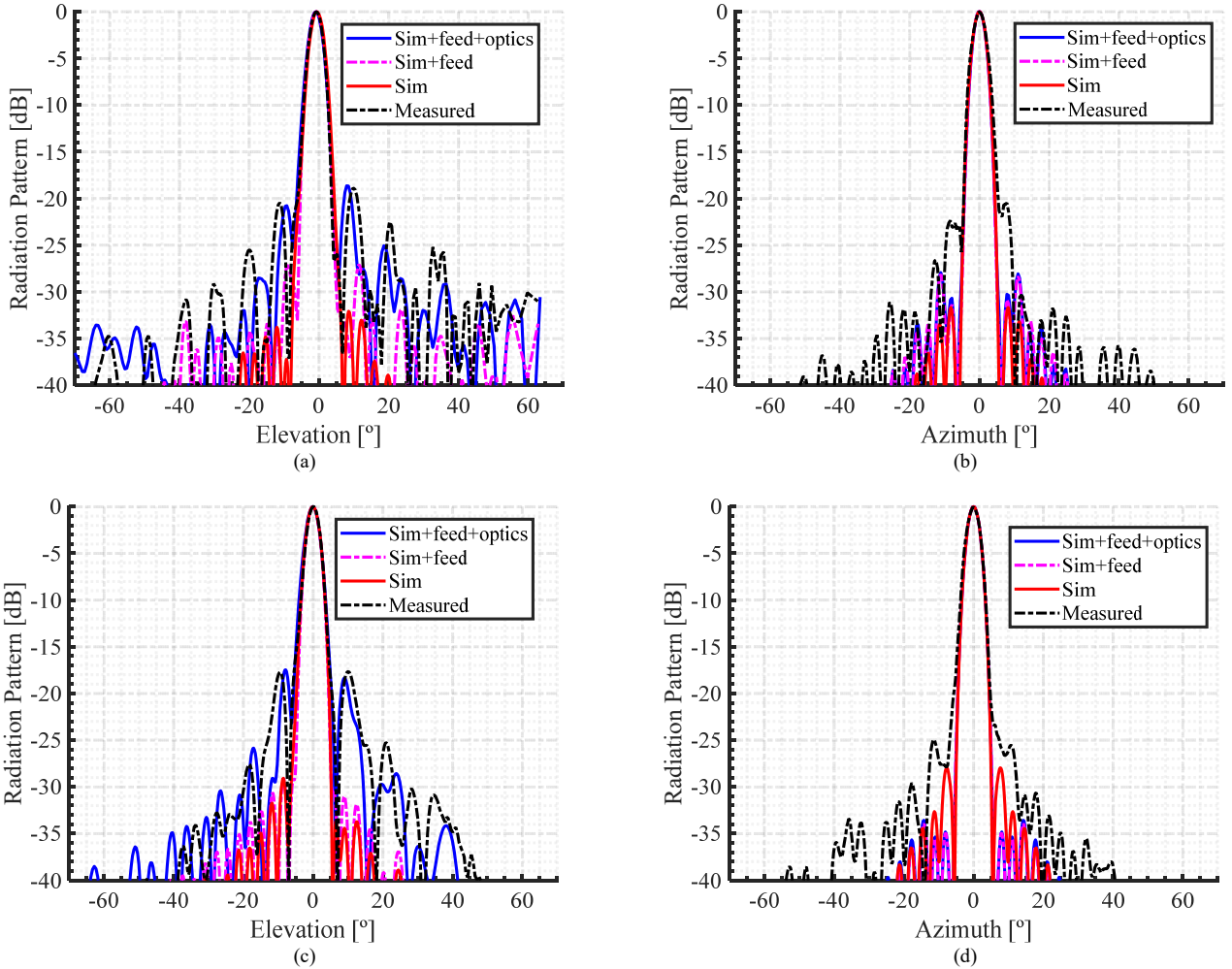
Fig. 10. Normalized radiation pattern at 28 GHz measured (dotted **black**) and simulated, considering the ideal model (solid **red**), the effect of the feed (dotted **purple**) and both the feed effect and the geometry errors (solid **blue**). Elevation (a) and Azimuth (b) cuts for the MFRAX. Elevation (c) and Azimuth (d) cuts for the MFRAY.

especially at frequencies below 28 GHz. In the azimuth cut, the evolution in-band for multi-faceted and single facet designs is different. According to this, both MFRAs have higher SLL than the SFRA. Constructive interference between the radiated field of each panel can generate these higher side lobe values since in the design of the MFRAs only the direction of pointing is considered. According to Table I, the SLL in the MFRAs is higher than the SFRA at 28 GHz, although in-band these values in all the designs are similar. The higher level of side lobes in the MFRAs in this cut is explained in detail in section V.

Table I shows the cross-polar level (XP) in the direction of maximum radiation, relative to the maximum copolar gain. All designs show higher purity polarization, with values above 30 dB of cross-polar discrimination in the entire band analyzed. The SFRA shows lower cross-polar values than the MFRAs around the design frequency, but at extreme frequencies, XP levels in the SFRA tend to be equal to or even higher than those obtained in the MFRAs. The superposition of the radiated field in each panel and the misalignments of the mechanical structure are possible reasons for the lower cross-polar isolation in the MFRAs around the design frequency. Comparing the two

multi-faceted prototypes, the MFRAY has higher cross-polar discrimination than MFRAX in the entire band, especially at frequencies below 28 GHz. The aperture efficiency has also been calculated for all designs, considering the spillover and the illumination (taper) on the reflectarray surfaces [1]. The MFRAs show an improvement in the aperture efficiency of about 3% concerning the SFRA in the whole band. The small differences in efficiency between the two multi-faceted structures are produced by the different illumination of the feed on each polarization. All reflectarrays achieve practically the same gain value at the design frequency and in the band analyzed.

V. ANALYSIS OF DISCREPANCIES.

Some differences are observed between the measured and simulated radiation patterns in the multi-faceted reflectarrays. These mismatches appear especially in the elevation cut (see Fig. 10(a), (c)) where the measured radiation pattern shows a higher field level outside beam than predicted in simulation. In this sense, a study is carried out to evaluate the discrepancies between the prototypes measured and the reflectarray model

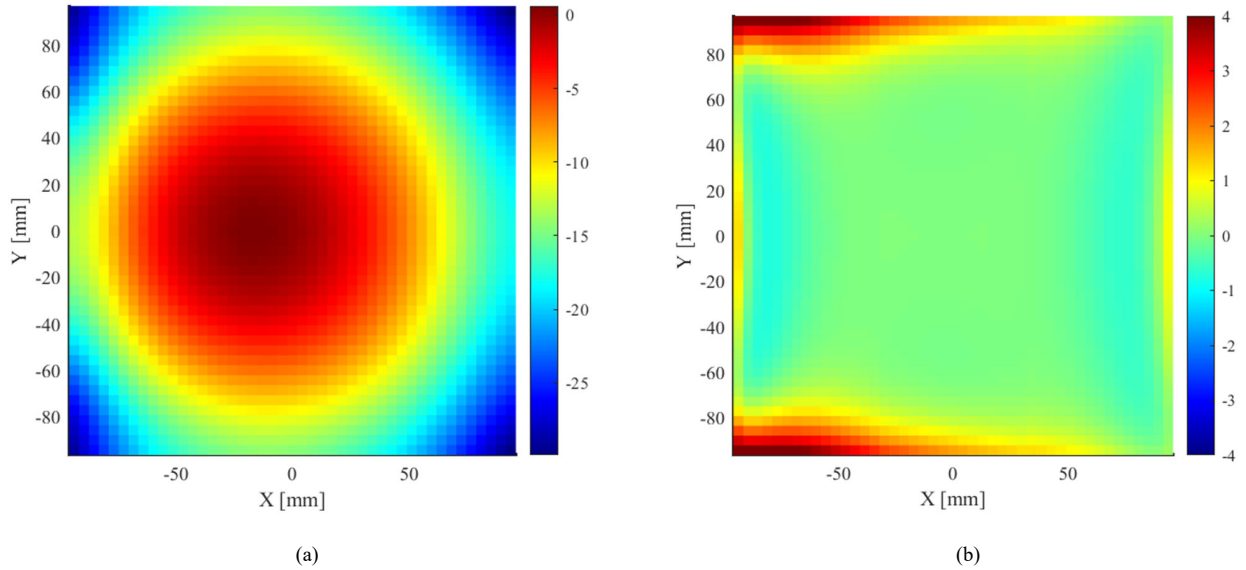(a)   (b)

Fig. 11. Incident field in the MFRAX surface considering the feed as a horn antenna model using GRASP [34] software: (a) Normalized incident field [dB]; (b) Difference [dB] with regard to the incident field considering the cos-q model, evaluated as $E_{GRASP} - E_{cosq}$.

simulated. During the process, two main sources of error are identified: the effect of using a real horn and the misalignments in the reflectarray structure.

A. Feed effect.

The horn antenna generates two effects on the reflectarray radiation pattern that affects both the multi-faceted reflectarrays and SFRA. The $\cos^q \theta$ model considered in the design does not fit perfectly with the real radiation pattern of the feed. This mismatch has an impact on the incident field considered during the analysis process. Fig. 11(a) shows the incident field on the MFRAX at 28 GHz considering a more realistic model of the horn antenna, using the GRASP software [34]. Fig. 11 (b) shows the difference between this incident field and what was used during the design process. It can be seen that the error between both models is small in most of the reflectarray surface.

Conversely, the measured field corresponds to the sum of the field radiated by the reflectarray structure and the radiation pattern of the feed. The contribution of the feed in the antenna margin of view corresponds to the back radiation of the horn antenna. Therefore, field values are much lower than those produced by the reflective structure (at least 35 dB below the field generated by the reflectarray). However, this back radiation produces interference patterns, which increases the field level outside the main beam, especially in elevation angles above 20º. This effect can be seen in Fig. 9 (a), (c) and (d) for each design respectively. The MFRAY is less sensitive to these effects due to the orientation of the feed with regard to the reflectarray structure.

Fig. 10 shows the simulated farfield of the multi-faceted structures considering the mentioned feed effects. A better agreement between simulation and measurements is achieved in the elevation cut, in comparison with the ideal simulation.

B. Impact of panel misalignment

Another source that generates discrepancies is the optics of the multi-faceted structure. Small errors in the relative positioning and orientation between panels are produced in the assembly of the antenna and they can generate slight antenna defocusing.

In the multi-faceted reflectarrays setup of Fig. 8, a gap between panels of 1 mm has been identified and the side panels have a deviation error of up to 1.5º in the tilt angle regarding the central one.

These geometrical errors are considered in the simulation along with the effects from the feed as can be seen in Fig. 10. Errors in the antenna optics increase the level of the side lobes, although they do not affect the width of the main lobe. After adding these error sources, a better agreement between measured and simulated results is achieved in the elevation cut in both multi-faceted results. In the azimuth cut, no significant improvement in simulation results is obtained because of the panel alignment uncertainties, since the division in panels is carried out just in the offset plane. Misalignment errors have an impact on the radiation pattern, especially in the SLL. However, it should be noted that errors in the optics of antennas onboard a satellite are expected to be smaller since they are an important concern for such applications [16],[17].

VI. BROADBAND PERFORMANCE.

Fig. 12 shows the gain of the prototypes measured over the entire Ka-band (26.5 – 40 GHz). The gain study is limited to this band because it is the frequency range where the probe is calibrated. Regarding the comparison between SFRA and MFRAs, the gain levels in the SFRA decrease rapidly when the frequency increases, while both multi-faceted structures remain the gain above 29 dBi in the entire band.

The band improvement of the multi-faceted structures is also evident in other parameters of the antenna . Table II shows some parameters of the radiation pattern in the SFRA and
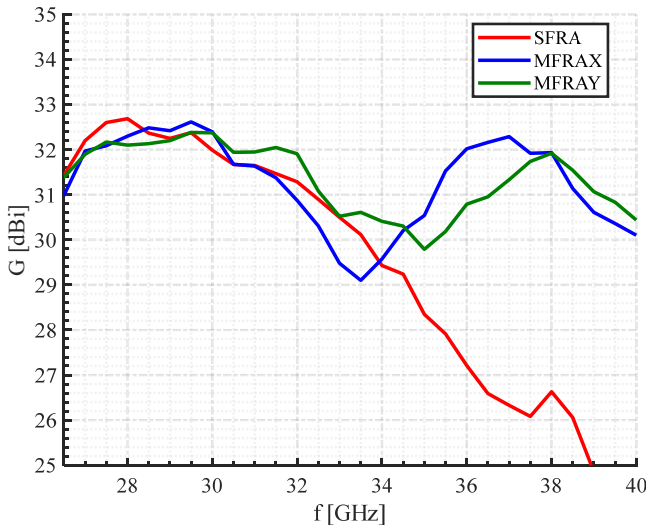
Fig. 12. Copolar gain measured in the Ka-band (26.5 – 40 GHz) for multi-faceted (MFRAX, MFRAY) and single facet (SFRA) designs.

TABLE II. ANTENNA RF PERFORMANCE. RANGE 37 - 39 GHz

		SFRA			MFRAX		
Frequency [GHz]		28.0	38.0	39.0	28.0	38.0	39.0
HPBW [º]	Az	3.9	7.4	6.7	4.8	4.8	4.6
	El	4.1	7.1	6.8	4.0	2.8	3.0
SLL [dB]	Az	-26.6	-10.0	-7.5	-20.9	-14.3	-10.6
	El	-26.0	-13.0	-9.8	-19.0	-14.2	-17.3
XP [dB]		-46.5	-40.0	-39.0	-30.0	-35.0	-32.0

MFRAX at 28 GHz and at upper frequencies of the Ka-band (38 and 39 GHz). At high frequencies, SFRA shows a Half Power Beam Width (HPBW) broader than that obtained at 28 GHz, which means a significant loss in antenna gain. In contrast, the MFRAX maintains HPBW values similar to those obtained at design frequency in azimuth, and slightly lower in elevation. In both prototypes, SLL values increase at upper frequencies regarding the SLL achieved at 28 GHz. However, this behavior is more relevant in the SFRA case, which reaches values higher than -10 dB. The crosspolar levels in the direction of maximum radiation remain below -30 dB in both prototypes.

To quantify the band improvement achieved in the MFRAs, the bandwidth as a function of the 1-dB drops of the gain measured at 28 GHz in the single facet is 3.5 GHz (27.0-30.5 GHz), which corresponds to 12.5% of f_0. Under the same conditions, the bandwidth in the MFRAX is 4.5 GHz (27.0 – 31.5), which corresponds to 16.1% of f_0, and the bandwidth in the MFRAY is 6.0 GHz (26.5 – 32.5 GHz), which corresponds to 21.4% of f_0. Both multi-faceted structures achieve at least a bandwidth enhancement of 30% with regard to the bandwidth achieved in the SFRA.

VII. CONCLUSIONS

A multi-faceted reflectarray panelized in 1-D is presented to overcome partially the spatial phase delay effect that limits the bandwidth in conventional printed reflectarrays. The antenna structure is a single-offset configuration composed of several panels, with different angular orientations, to conform a cylindrical parabolic reflector. In a SmallSat context, the multi-faceted structure can be stowed in the spacecraft body and easily deployed once the satellite is in orbit. To evaluate the performance, two multi-faceted reflectarrays are designed, manufactured, and tested at 28 GHz in linear polarization to collimate a high-gain pencil beam. The multi-faceted designs are compared with a single facet reflectarray of equivalent aperture.

The multi-faceted demonstrators achieve a better behavior in-band in the sectorization axis compared to a single facet design, with better stability of the main beam around 6 GHz of the working frequency. This enhancement in the radiation pattern is also in agreement with other parameters of the antenna such as more stability of the cross-polar and higher aperture efficiency. Moreover, the behaviour of the cell at upper frequencies of the Ka-band and the reduction of the spatial phase delay makes the multi-faceted structures achieve good performance in the entire Ka-band, with gain levels of about 30 dB or more and a ripple of about 3 dB. This means a significant bandwidth improvement with regard to the single facet version. The antenna performance in both multi-faceted prototypes is similar, which demonstrates the ability of these antennas to work in dual-polarization, either linear or circular depending on the unit cell that composed the panels.

Good agreement between measu rements and simulations is achieved in all designs but some discrepancies are shown in the multi-faceted patterns. In this sense, an analysis of discrepancies was carried out, where it has been identified two main sources of error that degrade the diagram pattern achieved: the effects of the feed and the errors in the optics of the setup. The errors identified in the supporting structure, degrade the radiation pattern of the multifaceted antennas. Although the alignment is an important concern in the implementation, the errors in the antenna optics onboard a satellite are expected to be smaller.

This work demonstrates the good performance of multi-faceted reflectarray structures. The use of different angular orientations in each panel, makes them exploit the unit cell and the optics of the antenna efficiently, improving the bandwidth of conventional printed reflectarrays while maintaining the low-profile, low-loss, low-cost, and polarization capabilities of these antennas.

REFERENCES

[1] J. Huang and J. A. Encinar, "Reflectarray antennas", *Jhon Wiley & Sons*, Hoboken, NJ USA, 2008, ISBN: 978-0-470-08491-5.

[2] E. Martinez-de-Rioja, A. F. Vaquero, M. Arrebola, E. Carrasco, J. A. Encinar and M. Achour, "Passive dual-polarized shaped-beam reflectarrays to improve coverage in millimeter-wave 5G networks", in *Proc. 15th European Congress on Antennas and Propagation (EuCAP), 2021*, pp. 1-5, doi: 10.23919/EuCAP51087.2021.9411196.

[3] H. Chou, T. Hung, N. Wang, H. Chou, C. Tung, and P. Nepa, "Design of a near-field focused reflectarray antenna for 2.4 GHz RFIDreader applications," in *IEEE Transactions on Antennas and Propagation*, vol. 59, no. 3, pp. 1013-1018, March 2011, doi: 10.1109/TAP.2010.2103030.

[4] Á. F. Vaquero, M. Arrebola, M. R. Pino, R. Florencio, and J. A. Encinar, "Demonstration of a reflectarray with near-field amplitude and phase constraints as compact antenna test range probe for 5G new radio devices," in IEEE Transactions on Antennas and Propagation, vol. 69, no. 5, pp. 2715-2726, May 2021, doi: 10.1109/TAP.2020.3030969.

[5] W. A. Imbriale, S. Gao, L. Boccia, Space antenna handbook, *Jhon Wiley & Sons, Hoboken*, 2012, ISBN: 978-1-119-94514-7.

[6] O. Kiris, K. Topalli, and M. Unlu, "A reflectarray antenna using hexagonal lattice with enhanced beam steering capability," in IEEE Access, vol. 7, pp. 45526-45532, 2019, doi: 10.1109/ACCESS.2019.2909313.

[7] P. Nayeri, F. Yang and A. Z. Elsherbeni, "Design and experiment of a single-feed quad-beam reflectarray antenna," in *IEEE Transactions on Antennas and Propagation*, vol. 60, no. 2, pp. 1166-1171, Feb. 2012, doi: 10.1109/TAP.2011.2173126.

[8] D. Martinez-De-Rioja, E. Martinez-De-Rioja, J. A. Encinar, R. Florencio and G. Toso, "Reflectarray to generate four adjacent beams per feed for multispot satellite antennas," in IEEE Transactions on Antennas and Propagation, vol. 67, no. 2, pp. 1265-1269, Feb. 2019, doi: 10.1109/TAP.2018.2880117.

[9] P. Nayeri, F. Yang and A. Z. Elsherbeni, "Design of single-feed reflectarrays with asymmetric multi-beams," *Proceedings of the 2012 IEEE International Symposium on Antennas and Propagation*, 2012, pp. 1-2, doi: 10.1109/APS.2012.6348725.

[10] J. A. Encinar *et al.*, "Dual-polarization dual-coverage reflectarray for space applications," in *IEEE Transactions on Antennas and Propagation*, vol. 54, no. 10, pp. 2827-2837, Oct. 2006, doi: 10.1109/TAP.2006.882172.

[11] D. R. Prado, J. A. López Fernández, M. Arrebola, M. R. Pino and G. Goussetis, "General framework for the efficient optimization of reflectarray antennas for contoured beam space applications," in *IEEE Access*, vol. 6, pp. 72295-72310, 2018, doi: 10.1109/ACCESS.2018.2882271.

[12] J. A. Encinar, M. Arrebola, L. F. de la Fuente and G. Toso, "A transmit-receive reflectarray antenna for direct broadcast satellite applications," in *IEEE Transactions on Antennas and Propagation*, vol. 59, no. 9, pp. 3255-3264, Sept. 2011, doi: 10.1109/TAP.2011.2161449.

[13] Imaz-Lueje, B., Prado, D.R., Arrebola, M. *et al.*, "Reflectarray antennas: a smart solution for new generation satellite mega-constellations in space communications". *Sci. Rep.* 10, 21554 (2020). https://doi.org/10.1038/s41598-020-78501-0 .

[14] J. Huang, "The development of inflatable array antennas," in IEEE Antennas and Propagation Magazine, vol. 43, no. 4, pp. 44-50, Aug. 2001, doi: 10.1109/74.951558.

[15] Martinez-de-Rioja, E.; Martinez-de-Rioja, D.; López-Sáez, R.; Linares, I.; Encinar, J.A. "High-efficiency polarizer reflectarray antennas for data transmission links from a cubesat". *Electronics* 2021, 10, 1802.

[16] R. E. Hodges, N. Chahat, D. J. Hoppe and J. D. Vacchione, "A Deployable high-gain antenna bound for mars: developing a new folded-panel reflectarray for the first Cubesat mission to Mars.," in *IEEE Antennas and Propagation Magazine*, vol. 59, no. 2, pp. 39-49, April 2017, doi: 10.1109/MAP.2017.2655561.

[17] R. E. Hodges, M. J. Radway, A. Toorian, D. J. Hoppe, B. Shah, and A. E. Kalman, "ISARA - Integrated Solar Array and Reflectarray CubeSat deployable Ka-band antenna," *2015 IEEE International Symposium on Antennas and Propagation & USNC/URSI National Radio Science Meeting*, 2015, pp. 2141-2142, doi: 10.1109/APS.2015.7305460.

[18] E. Cote Pelletier, C. Mireault-Lecourt and J. -J. Laurin, "Reflectarray antenna concept for a snow mass measurement sar mission in Ku-band on a nanosatellite platform," in *IEEE Antennas and Wireless Propagation Letters*, doi: 10.1109/LAWP.2021.3113798.

[19] R. E. Hodges, J. C. Chen, M. R. Radway, L. R. Amaro, B. Khayatian and J. Munger, "An extremely large Ka-band reflectarray antenna for interferometric synthetic aperture radar: enabling next-generation satellite remote sensing," in *IEEE Antennas and Propagation Magazine*, vol. 62, no. 6, pp. 23-33, Dec. 2020, doi: 10.1109/MAP.2020.2976319.

[20] J. Huang, "Bandwidth study of microstrip reflectarray and a novel phase reflectarray concept," in *Antennas and Propagation Society Intl. Symp. 1995*, AP-S. Digest, pp.582-585, June 1995.

[21] J. A. Encinar and J. A. Zornoza, "Broadband design of three-layer printed reflectarrays," in *IEEE Transactions on Antennas and Propagation*, vol. 51, no. 7, pp. 1662-1664, July 2003, doi: 10.1109/TAP.2003.813611.

[22] L. Moustafa, R. Gillard, F. Peris, R. Loison, H. Legay, and E. Girard, "The Phoenix Cell: a new reflectarray cell with large bandwidth and rebirth capabilities," in *IEEE Antennas and Wireless Propagation Letters*, vol. 10, pp. 71-74, 2011, doi: 10.1109/LAWP.2011.2108633.

[23] E. Carrasco, J. A. Encinar and M. Barba, "Wideband reflectarray antenna using true-time delay lines," *The Second European Conference on Antennas and Propagation*, EuCAP 2007, 2007, pp. 1-6, doi: 10.1049/ic.2007.0939.

[24] D. R. Prado, M. Arrebola, M. R. Pino and G. Goussetis, "Broadband reflectarray with high polarization purity for 4K and 8K UHDTV DVB-S2," in IEEE Access, vol. 8, pp. 100712-100720, 2020, doi: 10.1109/ACCESS.2020.2999112.

[25] D. Martinez-de-Rioja et al., "Transmit–receive parabolic reflectarray to generate two beams per feed for multispot satellite antennas in ka-band," in *IEEE Transactions on Antennas and Propagation*, vol. 69, no. 5, pp. 2673-2685, May 2021, DOI: 10.1109/TAP.2020.3030942.

[26] Greco, F., Boccia, L., Arnieri, E., Amendola, G., "A Ka-Band cylindrical paneled reflectarray antenna" in Electronics 2019, 8, 654. https://doi.org/10.3390/electronics8060654

[27] Legay, Hervé & Bresciani, Daniele & labiole, eric & Chiniard, R. & Gillard, R. (2013). "A multi facet composite panel reflectarray for a space contoured beam antenna in Ku band" in *Progress In Electromagnetics Research B*. 54. 1-26. DOI: 10.2528/PIERB13061407.

[28] Borja Imaz-Lueje, Daniel R. Prado, Manuel Arrebola, Marcos R. Pino, "Design of an offset multi-faceted reflectarray antenna" in *15th European Conference on Antennas and Propagation*, March 2021.

[29] E. Carrasco, M. Barba, J. A. Encinar, M. Arrebola, F. Rossi and A. Freni, "Design, manufacture, and test of a low-cost shaped-beam reflectarray using a single layer of varying-sized printed dipoles," in IEEE Transactions on Antennas and Propagation, vol. 61, no. 6, pp. 3077-3085, June 2013, doi: 10.1109/TAP.2013.2254431.

[30] R. Florencio, R. R. Boix and J. A. Encinar, "Design of a reflectarray antenna at 300 GHz based on cells with three coplanar dipoles," 2013 IEEE Antennas and Propagation Society International Symposium (APSURSI), 2013, pp. 1350-1351, doi: 10.1109/APS.2013.6711335.

[31] R. Florencio, R. R. Boix, E. Carrasco, J. A. Encinar, and V. Losada, "Efficient numerical tool for the analysis and design of reflectarrays based on cells with three parallel dipoles," in *Microw. Opt. Technol. Lett.*, vol. 55, no. 6, pp. 1212-1216, Jun.2013. DOI: https://doi.org/10.1002/mop.27533

[32] W. L. Stutzman, G. A. Thiele, "Antenna theory and design", 3rd Edition, *Jhon Wiley & Sons*, Hoboken, NJ USA, 2008, ISBN: 978-0-470-57664-9.

[33] TICRA: SNIFT | Spherical Near-field to Far-field Transformation Software. Available: https://www.ticra.com/software/snift/

[34] TICRA: GRASP | Reflector Antenna Design Software. Available: https://www.ticra.com/software/grasp/
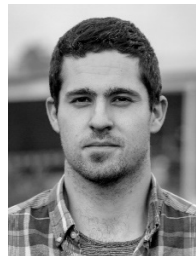
BORJA IMAZ-LUEJE (Student Member, IEEE) was born in Riaño, Asturias, Spain, in 1995. He received the B. Sc. And M. Sc. Degrees in telecommunications engineering from the Universidad de Oviedo at Gijón, Spain, in 2017 and 2019, respectively, where is currently pursuing the Ph. D. degree.

Since 2016, he has been a Research Assistant with the Signal Theory and Communications Area, Universidad de Oviedo. From 2018 to 2019, he spent several months in a fellowship in Rohde & Schwarz GmbH & Co KG, Munich, Germany, where he was involved in the deployment of CATR systems and OTA measurements. His currently research interests include the development of efficient analysis and design techniques of reflectarrays in complex configurations, working in environments of near- and farfield.

MARCOS R. PINO received the M.Sc. and Ph.D. degrees in telecommunication engineering from the University of Vigo, Spain, in 1997 and 2000, respectively.

In 1998, he was a Visiting Scholar with the ElectroScience Laboratory, The Ohio State University, Columbus, OH, USA. From 2000 to 2001, he was an Assistant Professor with the University of Vigo. Since 2001, he has been with the Electrical Engineering Department, University of Oviedo at Gijón, Spain, where he is currently Full Professor, teaching courses on communication systems and antenna design. From 2017 to 2019, he has spent several months as Visiting

Fellow with the Department of Information Engineering, University of Pisa, Italy, collaborating in near-field UHF-RFID applications.

His current research interests include antenna design optimized for both near-field and far-field applications, antenna measurement techniques, and efficient computational techniques applied to EM problems.

MANUEL ARREBOLA (Senior Member, IEEE) was born in Lucena, Córdoba, Spain. He received the M.Sc. degree in telecommunication engineering from the University of Málaga, Málaga, Spain, in 2002, and the Ph.D. degree from the Technical University of Madrid (UPM), Madrid, Spain, in 2008.

From 2003 to 2007, he was a Research Assistant with the Department of Electromagnetism and Circuit Theory, UPM. In 2005, he was a Visiting Scholar with the Department of Microwave Techniques, Universität Ulm, Ulm, Germany. In 2007, he joined the Department of Electrical Engineering, University of Oviedo at Gijón, Spain, where he is currently an Associate Professor. In 2009, he was with the European Space Research and Technology Centre, European Space Agency, Noordwijk, The Netherlands, for two months. In 2018, he was a Visiting Professor with the Edward S. Rogers Sr. Department of Electrical and Computer Engineering, University of Toronto, Toronto, ON, Canada. In 2019, he was a Visiting Professor with the Institute of Sensors, Signals and Systems, Heriot-Watt University, Edinburgh, U.K. His current research interests include the development of efficient analysis, design, and optimization techniques of reflectarray and transtmitarray antennas both in near- and far-fields.

Dr. Arrebola was a co-recipient of the 2007 S. A. Schelkunoff Transactions Prize Paper Award by the IEEE Antennas and Propagation Society.